XMM-Newton Calibration Technical Note

Empirical correction of the EPIC effective area based on *NuSTAR* observations

Felix Fürst

April 5, 2022

1 Introduction & Background

Calibration of the effective area for X-ray telescopes is a long-standing issue in the community. The lack of proper standard candles in the X-ray sky means that X-ray telescopes have to largely rely on ground calibration data. However, the in-orbit effective area might deviate from the measurements on the ground and is likely to change over time. Therefore efforts are made to establish at least a good cross-calibration between currently operating X-ray telescopes, to allow the use of data from different instruments together.

These cross-calibration efforts are now largely coordinated by the International Astrophysical Consortium for High Energy Calibration (IACHEC). Madsen et al. (2017a) present the most recent results from these efforts, where they compare the photon index and flux between *XMM-Newton*, *Chandra*, *Suzaku*, *Swift*, and *NuSTAR* using two well known calibration sources, 3C 273 and PKS 2155−304. This investigation shows that *XMM-Newton* EPIC-pn typically measures a significantly lower flux and slightly different spectral slope than other X-ray instruments.

In particular, differences between the implied spectral parameters of EPIC-pn and *NuSTAR* are evident. Based on results documented in the wider scientific literature, the SOC performed a detailed study based on a sample of simultaneous observations between *XMM-Newton* and *NuSTAR* (Gokus et al., 2016; Gokus, 2017). The results showed indeed a systematic difference in spectral slope and shape between EPIC-pn and the *NuSTAR* detectors. This discrepancy is in particular unfortunate as a large fraction of the *XMM-Newton* observations are nowadays coordinated with *NuSTAR*, often even simultaneous. An update to the effective area of one or both instruments is therefore required, to increase the scientific output and reliability of the joint observations.

To improve on the cross-calibration it is best to observe and model a source with a simple spectrum, e.g., a pure power-law, to eliminate as many astrophysical uncertainties as possible. One well studied power-law source is the Crab Nebula (M1). The Crab is observed regularly simultaneously by *XMM-Newton* and *NuSTAR* about every 6 months for timing calibration purposes. In this TN we use the spectra from those simultaneous observations to find an empirical correction function to the EPIC-pn ARF that recovers the slope and shape of the expected pure power-law better and reaches a higher degree of agreement with *NuSTAR*. These

corrections will then also be applied to the MOS effective areas, to keep the agreement between all EPIC detectors.

In addition to differences in the spectral shape, EPIC-pn fluxes are significantly lower than the *NuSTAR* fluxes (Madsen et al., 2017a; Gokus, 2017). This discrepancy has increased with the release of *NuSTAR* CALDB v20211020 in which the *NuSTAR* ARF and vignetting function was updated. With this calibration compared to the EPIC-pn effective area calibration (`XRT3_XAREAEF_0013.CCF`), typical flux discrepancies are on the order of ∼20%. Without further knowledge it is unclear which instrument recovers the true astrophysical fluxes better, i.e., which effective area description is closer to the real effective area of the respective telescope.

The rest of the TN is structured as follows: in Sect 2 we outline in detailed the methods used and assumptions taken during the modeling stage. In Sect. 3 we evaluate and test the proposed correction using a database of simultaneous *XMM-Newton* and *NuSTAR* observation. In Sect. 4 we show the final results and describe how they can be applied by the user. In Sect. 5 we provide a brief outlook to further updates for the EPIC effective area.

2 Method

2.1 Software and Calibration versions

All *XMM-Newton* data were extracted using SAS 19.1.0 with CCF files as of 2021-07-27. *NuSTAR* data were extracted with HEASOFT v6.29b and `nupipeline` v2.1.1 with CALDB v20211020 as well as CALDB v20210908 to assess the impact of the large change in v20211020. Data analysis was mainly performed with the Interactive Spectral Interpretation System (ISIS) v1.6.2-47 (Houck, 2002). If not otherwise stated uncertainties are reported at the 90% level. All fits were obtained by minimizing χ^2.

2.2 Crab data

We analysed all Crab observation taken simultaneously between *XMM-Newton* and *NuSTAR* between 2013 and August 2021. A detailed observation log is given in Table 1.

The EPIC-pn data were taken in burst mode with the thick filter, in which the rows in CCD4 are shifted very fast during the science exposure, allowing for a very high time-resolution and mitigating pile-up even for the brightest sources(Kirsch et al., 2006; Kuster et al., 1999). After the fast shift, a standard slow read-out of the CCD is performed to gather the data. In this case the 20 rows around the bore-sight are ignored, as they are expected to be heavily piled-up. This two-step exposure process leads to a duty cycle of only 3%. We extract the source spectrum from the full width of the chip (64 pixels). Because the source dominates the whole width of the chip, a background spectrum cannot be extracted, but the background is negligible given the high count-rate of the source.

While all spatial information along the y-direction (shift direction) is lost, still the whole CCD4 chip is exposed to the sky and collects photons during the exposure. As the Crab is extended and the spectrum is spatially variable, we made sure to extract the exact same region as the CCD4 footprint on the sky from *NuSTAR*. An example of these regions are given in Fig 1. The figure also shows a typical *NuSTAR* background region, although the background contribution can be ignored for our energy ranges of interest.

Given the shape of the extraction region and the fact that the Crab nebula is extended, we chose to calculate the *NuSTAR* ARF based on the extended ARF algorithm using an equal weighing across the whole region. Because this might not recover the real effective area exactly and does

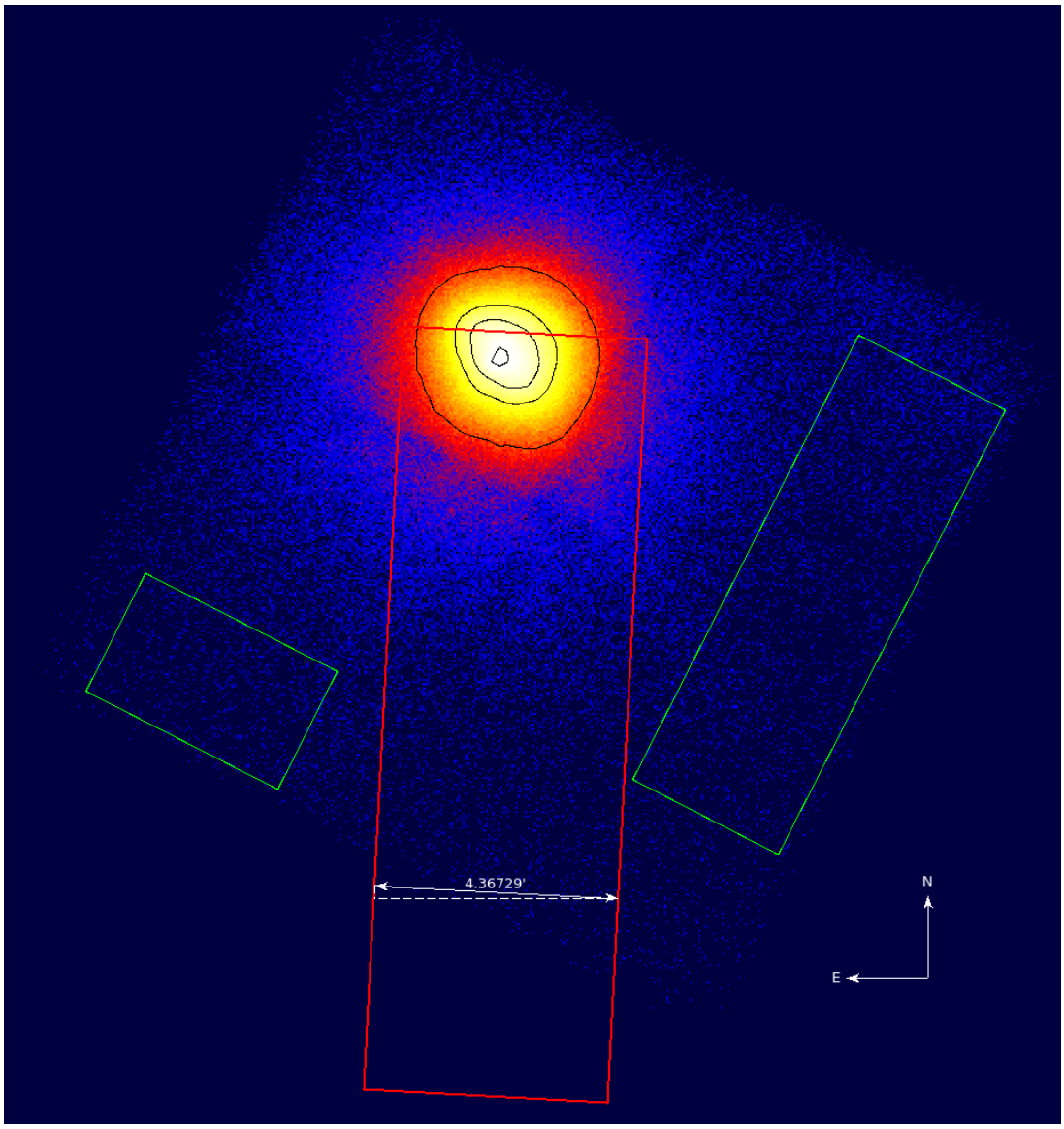

Figure 1: Sky image from *NuSTAR* FPMA of ObsID 10502001008, superimposed with the source extraction region (red) and the background regions (green). The black contours are based on the *NuSTAR* image to show the extend and center of the Crab nebula. The source extraction region corresponds to the footprint of *XMM-Newton*EPIC-pn CCD4 on the sky.

Table 1: Observation Log for the Crab observations. The EPIC-pn data were fitted in the 3–12 keV range, while the *NuSTAR* data were fitted between 5–50 keV.

	ObsID		Exposure [s]		Photon index Γ	
Date	XMM	NuSTAR	EPIC-pn	NuSTAR	EPIC-pn	NuSTAR
2013-09-03	0611182101	10002001004	449.12	2386.58	2.032 ± 0.011	2.087 ± 0.004
2014-10-02	0611182501	10002001008	384.37	4941.78	2.039 ± 0.014	2.0892 ± 0.0022
2017-09-28	0793980301	10302001004	336.61	7547.15	2.026 ± 0.014	2.0958 ± 0.0022
2018-03-14	0811022501	10402001008	838.71	5657.87	1.984 ± 0.009	2.0556 ± 0.0022
2018-09-11	0811022701	10402001010	265.96	1133.58	$2.005^{+0.016}_{-0.015}$	2.101 ± 0.005
2018-09-12	0811022801	10402001012	767.95	1270.67	2.043 ± 0.011	2.104 ± 0.005
2018-09-13	0811022901	10402001016	999.04	1169.16	2.041 ± 0.009	2.106 ± 0.005
2019-03-11	0811023101	10502001008	264.85	2417.62	1.977 ± 0.016	2.054 ± 0.004
2019-08-30	0811023301	10502001015	145.32	7492.19	2.044 ± 0.020	2.1069 ± 0.0019
2020-02-27	0811023601	10602002002	296.03	3567.71	1.967 ± 0.015	2.0590 ± 0.0029
2020-08-29	0811023801	10602002008	206.75	2514.66	2.033 ± 0.016	2.105 ± 0.004
2021-02-24	0811024101	10702303004	310.64	3150.43	1.987 ± 0.015	2.0626 ± 0.0030
2021-08-29	0811024301	10702303008	229.12	3891.06	2.037 ± 0.016	2.1133 ± 0.0027

not correspond exactly to the EPIC-pn area exposed to the sky, we expect larger offsets between the absolute normalization between EPIC-pn and *NuSTAR*.

The importance of lining up the extraction region between EPIC-pn and *NuSTAR* is clearly seen by the fact that the measured photon-index is varying slightly but significantly with a period of 1 year ($\Delta\Gamma \approx 0.05$, see Table 1). As observations are taken every ∼6 months, the position angle is rotated by $\sim 180^\circ$ between them, which means that either only the northern or only the southern part of the nebula is covered (see Fig. 1 where only the southern part is covered). Through this rotation data from regions with different spectral index are taken (see, e.g., Madsen et al., 2017b), resulting in the observed changes. With our selection of regions we find a constant offset (within the uncertainties) between EPIC-pn and *NuSTAR* for all epochs.

2.3 Crab model fitting

We rebin all data to follow the energy resolution of the respective instrument and oversampling it by no more than a factor of 3 and also require a signal-to-noise ratio (S/N) of at least 3 per bin. We model EPIC-pn between 3–12 keV and the *NuSTAR* instruments between 5–25 keV. The higher energies in *NuSTAR* are necesssary to securely define the power-law index. Our base model is a simple `powerlaw` modified by galactic absorption modeled by the `tbnew` model (Wilms et al., 2000). We use the corresponding Wilms cross-sections and the abundances by Verner et al. (1996). Given that we start our fit only at 3 keV, we fixed the absorption column to $N_{\rm H} = 4 \times 10^{21}\,{\rm cm}^{-2}$, in line with previous *XMM-Newton* results (Kirsch et al., 2006).

We then fit all epochs simultaneously, requiring that each epoch has the same photon index between EPIC-pn, FPMA, and FPMB. However, we allow for different normalizations for all three instruments. While this approach results in a statistically acceptable fit, with $\chi^2 = 7305.2$ for 6185 degrees of freedom (d.o.f.) for a $\chi^2_{\rm red} = 1.18$, clear structures can be see in the stacked EPIC-pn residuals shown in Fig. 2a. Part of these residuals can be explained by the fact that we measure slightly different photon-indices for *XMM-Newton* and *NuSTAR* when fitting them individually (Table 1), however, the residuals clearly have a more complex shape then we would expect from just a difference in Γ.

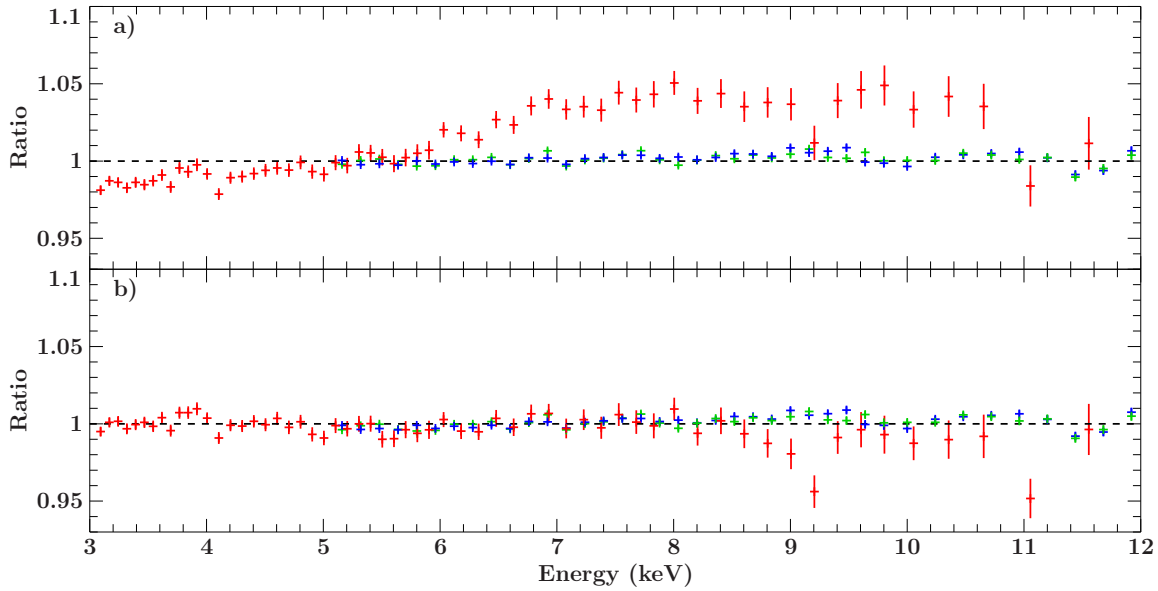

Figure 2: Stacked EPIC-pn (red) residuals, FPMA (blue), and FPMB (green) residuals of a joint fit to all Crab epochs, requiring the same photon index for all instrument in each epoch. *a)* Without any correction function for EPIC-pn. *b)* After applying the spline correction function.

To remove the structures in the residuals we model them with a simple cubic spline, anchored just below and above the EPIC-pn energy range in use. This spline describes the structure in the residuals very well and no more complicated models are necessary.

We use the multiplicative XSPEC model `spline` in which we set `Estart` to 1 keV, `Eend` to 12.5 keV, and `Ystart` to 1 while we allowed the three other parameters (`Yend`, `YPstart`, and `YPend`, i.e., the value and slope at the anchor points), to vary freely. We require that those three parameters are the same for all EPIC-pn spectra. We fixed `Ystart` to 1 to avoid any degeneracy with the normalization.

In addition to the parameters of the spline, each of the 10 epochs has four variable parameters, the power-law photon-index Γ and the normalization for each instrument. We have thus a model with 56 variable parameters. The statistical quality of the fit is excellent with $\chi^2 = 6260.5$ for 6183 d.o.f. ($\chi^2_{\rm red} = 1.01$).

We show the residuals after applying the spline correction function in Fig. 2b and the correction function itself in Fig. 3. To calculate uncertainties on the correction function, we ran a Markov-Chain Monte Carlo (MCMC) simulations, based on the `emcee` algorithm (Goodman & Weare, 2010; Foreman-Mackey et al., 2013). We used 12 walkers for each of the 56 variable parameters and let them run for 5000 steps. Before using the results we discarded the first 1000 steps as burn-in period, after which all walkers have stabilized around a global minimum.

We then select 100 walkers randomly to plot an ensemble of possible correction functions within the 90% uncertainty contour of all parameters. This ensemble is plotted in Fig. 3 in gray. From that we also calculate the 90% quantile, i.e., 90% of the curves lie between the blue dashed lines in the Figure. As can be seen, the deviation is smaller than 1% over most of the energy range, only increasing slightly above 11 keV. The triangle plot of the `spline` parameters can be found in the appendix (Fig 8).

The corrections have been implemented in the new extension `ABSCORRAREA` of the CCF file `XRT3_XAREAEF_0014.CCF`. The correction can be applied with `arfgen` as of SAS v20.0 by setting

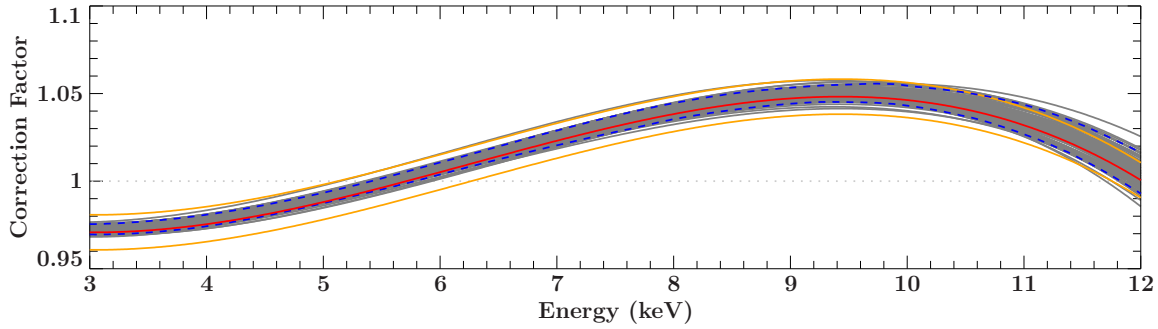

Figure 3: Spline correction function based on modeling of the Crab nebula. Note that the absolute value of the factor is arbitrarily chosen. In red the best-fit is shown, with the ±1% deviation in orange. In gray an ensemble of 100 solutions based on walkers within the 90% contour of an MCMC simulation are shown, with the corresponding 90% quantile of all walkers shown as a blue dashed line.

Table 2: Observation Log for the 3C 273 and 1ES 0229+200 observations.

	ObsID		Exposure [ks]		Parameters	
Date	XMM	NuSTAR	XMM	NuSTAR	Γ	$E_{\rm fold}$ [keV]
3C 273						
2012-07-16	0414191001	10002020001	17.23	244.00	$1.620^{+0.010}_{-0.009}$	$\left(1.98^{+0.30}_{-0.23}\right) \times 10^2$
2015-07-13	0414191101	10002020003	47.95	49.42	$1.682^{+0.015}_{-0.021}$	$\left(2.8^{+1.6}_{-1.0}\right) \times 10^2$
2016-06-26	0414191201	10202020002	43.84	35.42	$1.526^{+0.012}_{-0.014}$	$\left(1.47^{+0.25}_{-0.20}\right) \times 10^2$
2017-06-26	0414191301	10302020002	42.42	35.40	1.587 ± 0.014	$\left(1.64^{+0.44}_{-0.30}\right) \times 10^2$
2018-07-04	0414191401	10402020006	42.61	40.32	1.634 ± 0.022	$\left(1.5^{+0.6}_{-0.4}\right) \times 10^2$
2019-07-02	0810820101	10502620002	47.29	49.41	$1.675^{+0.020}_{-0.021}$	$\left(2.7^{+1.7}_{-0.9}\right) \times 10^2$
2020-07-06	0810821501	10602606002	47.63	44.02	$1.622^{+0.014}_{-0.017}$	$\left(1.6^{+0.5}_{-0.4}\right) \times 10^2$
1ES 0229+200						
2021-08-08	0810821801	10702609002	59.70	95.16	1.989 ± 0.023	33^{+7}_{-5}

the parameter `applyabsfluxcorr=yes`.

2.4 3C 273 model fitting

The AGN3C 273 has been used as calibration source for a long time and is observed on a roughly yearly cadence with *XMM-Newton* and *NuSTAR*. We use seven data-sets taken between July 2012 and July 2020, as detailed in Table 2. In addition we use one observation of 1ES 0229+200, which was observed in August 2021, also as part of an IACHEC campaign. For each observation we performed simple perliminary fits with an absorbed power-law with an exponential cutoff, to estimate spectral variability.

The *XMM-Newton* data were taken in Small Window mode of EPIC-pn, with either the Medium or the Thick filter, mitigating pile-up in the source. We carefully checked for pile-up effects, but found that even if mild pile-up is present in some observations, it does not influence the spectrum significantly. We also carefully checked for variability during the observation, and also find this to be negligible, and hence did not filter on strict simultaneous GTIs between *NuSTAR* and *XMM-Newton* to improve statistics. We extracted the source spectrum from a circular region with a radius of 36″, centered on the brightest pixel. We extracted the background spectrum

from as far away as the source as possible within the Small Window.

We extracted *NuSTAR* source spectra from a circular region with a radius of 90″, centered on the brightest pixel. Background spectra were extracted from a circular region with a radius of 160″ on the opposite site of the field-of-view, as the complete detector 0 quadrant was dominated by the source.

For 3C 273, we base our model on the model used by Madsen et al. (2015), describing the continuum with a `cutoffpl` plus a `diskbb` component. We find that a small contribution from reflection, i.e., an iron line and a Compton hump, is necessary in some spectra. We assume that this reflection is from distant reflection and constant over all epochs. We model the reflection with the `xillver` model (García et al., 2013) and fix the inclination to 35° and the iron abundance to solar. We set the redshift to $z = 0.158$ and assume neutral matter ($\log \xi = 0$). The continuum is model by a power-law model with an exponential cutoff at high energies (`cutoffpl`). We require that the photon-index and the high energy cutoff between the `cutoffpl` and the `xillver` model is the same. The continuum is modified by absorption at low energies, described by the `tbnew` model, using the same abundances and cross-sections as for the Crab. We fix the absorption column to $N_{\rm H} = 1.68 \times 10^{20}\,{\rm cm}^{-2}$. Additionally we allow for a small gainshift in the energy scale of the EPIC-pn, which results in offsets on the order of 10 eV.

Due to varying continuum strength and S/N, the reflection component cannot be measured in all epochs. We therefore fit for it using only epochs 2012, 2019, and 2020, which showed the largest improvement in the quality of fit when adding this component ($\Delta\chi^2 > 25$). We fit these three epochs simultaneously, allowing different continuum parameters in each epoch, but requiring the reflection component to be the same. We find a good fit with $\chi^2 = 2271$ for 1898 d.o.f. We find a normalization of the reflection component of $A_{\rm refl} = (4.2 \pm 0.7) \times 10^{-5}$.

For 1ES 0229+200, we fit the single epoch with and absorbed `cutoffpl` model (see, .e.g., Wierzcholska & Wagner, 2020). The spectrum does not require any additional components like a thermal blackbody component or reflection. With this model, we find a good fit with $\chi^2 = 375$ for 378 dof.

We then fix the reflection component for 3C 273 to the values found in the previous fit using the limited sample. We set the cross calibration constant of *NuSTAR* FPMA to 1.0 and allow for a variable cross-normalization to EPIC-pn and FPMB. We first perform the fit without the corrections and find an acceptable fit with $\chi^2 = 6130$ for 5440 dof. We then apply the correction as calculated in the previous sections based on the Crab data, which results in a significantly improved fit with $\chi^2 = 5772$ for the same number of free parameters. We find that the cross-calibration for EPIC-pn towards *NuSTAR*/FPMA is on average 0.81 ± 0.03, i.e., fluxes of EPIC-pn in the 3-12 keV energy band are almost 20% lower than of *NuSTAR*.

3 Testing

3.1 Small Window mode

We have checked the corrections proposed here using a large sample of AGN data using 22 observations, obtained simultaneously by *XMM-Newton* and *NuSTAR* (based on a pipeline developed by A. Joyce, priv. comm., `https://github.com/AmyJoyce43/XMM_scripts`). The list of sources and observations used can be found in the appendix (Table 4). All observations were performed in Small Window mode for EPIC-pn and rigorously checked for variability and pile-up. The spectra were fitted simultaneously between *XMM-Newton* and *NuSTAR*, using the 3–12 keV range in EPIC-pn and the 3–25 keV range in *NuSTAR* FPMA and FPMB. Phenomenological models were chosen to describe the spectra well, while using as few parameters

Table 3: Best-fit parameters for all 3C 273 epochs and the 1ES 0229+200 observation in 2021.

Parameter	2015	2016	2017	2018
$A_{\rm PL}$	$0.01716^{+0.00014}_{-0.00013}$	0.02889 ± 0.00018	0.01630 ± 0.00013	$0.01641^{+0.00016}_{-0.00015}$
$A_{\rm DBB}$	$\left(1.12^{+0.30}_{-0.22}\right) \times 10^3$	$\left(1.47^{+0.22}_{-0.19}\right) \times 10^3$	$\left(8.4^{+2.8}_{-2.0}\right) \times 10^2$	$\left(9.3^{+1.6}_{-1.3}\right) \times 10^2$
$T_{\rm in}$ [keV]	0.146 ± 0.007	$0.160^{+0.005}_{-0.004}$	0.150 ± 0.009	0.168 ± 0.006
Γ	1.697 ± 0.007	1.514 ± 0.005	1.573 ± 0.007	1.678 ± 0.008
$E_{\rm fold}$ [keV]	$\left(2.1^{+0.6}_{-0.4}\right) \times 10^2$	$\left(1.20^{+0.10}_{-0.09}\right) \times 10^2$	$\left(1.20^{+0.16}_{-0.13}\right) \times 10^2$	$\left(2.0^{+0.6}_{-0.4}\right) \times 10^2$
$CC_{\rm FPMB}$	0.962 ± 0.007	0.996 ± 0.006	0.987 ± 0.008	0.989 ± 0.008
GS [eV]	0.018 ± 0.004	$0.0131^{+0.0026}_{-0.0027}$	$(6 \pm 4) \times 10^{-3}$	$(6 \pm 4) \times 10^{-3}$

Parameter	2019	2020	2021 (1ES 0229+22)
$A_{\rm PL}$	$0.01490^{+0.00013}_{-0.00014}$	$0.01667^{+0.00014}_{-0.00015}$	$\left(3.01^{+0.06}_{-0.05}\right) \times 10^{-3}$
$A_{\rm DBB}$	$\left(7.4^{+1.1}_{-1.0}\right) \times 10^2$	$\left(1.27^{+0.19}_{-0.15}\right) \times 10^3$	—
$T_{\rm in}$ [keV]	0.175 ± 0.005	0.162 ± 0.005	—
Γ	$1.721^{+0.005}_{-0.007}$	1.644 ± 0.008	$2.015^{+0.025}_{-0.024}$
$E_{\rm fold}$ [keV]	$\left(4.99^{+0.00}_{-1.51}\right) \times 10^2$	$\left(1.56^{+0.30}_{-0.22}\right) \times 10^2$	30^{+6}_{-5}
$CC_{\rm FPMB}$	0.996 ± 0.008	1.008 ± 0.008	0.964 ± 0.021
GS [eV]	$(8 \pm 4) \times 10^{-3}$	$(8 \pm 4) \times 10^{-3}$	$\left(-6^{+7}_{-8}\right) \times 10^{-3}$
$CC_{\rm pn}$	—		
χ^2/dof	5079.32/4740		
$\chi^2_{\rm red}$	1.07		

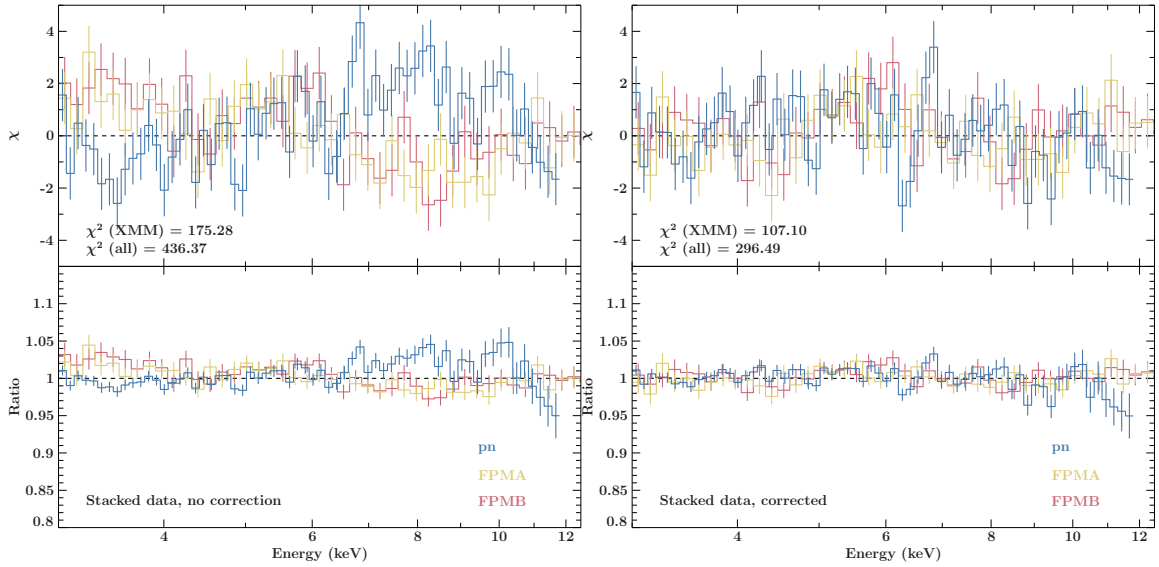

Figure 4: Residuals of the stacked best-fit models to the stacked data of 22 AGN spectra in terms of χ (top) and as ratio data/model (bottom). In blue the EPIC-pn residuals are shown, in red and yellow the *NuSTAR* FPMA and FPMB residuals, respectively. The left column shows the results for the non-corrected fits, the right column the results when using the new CCF. For details see text.

as possible. In practice, this means that most of them could be described by a powerlaw and a Gaussian emission line to model the Fe Kα line. A few spectra needed more complicated models to achieve a fit with $\chi^2 \approx 1$, including multiple lines, thermal disk components or reflection components. We allowed for cross-normalization constants between *NuSTAR* and EPIC-pn, and between the *NuSTAR* detectors. The fit was first performed with the old calibration and then a second with the updated calibration including the proposed corrections.

We then stacked all data and their respective best-fit models to calculate the residuals and fit quality, as shown in Fig. 4. We find that for EPIC-pn only, the fits with the new CCF provide an improvement of $\Delta\chi^2 = 68.18$ over the not corrected data, while the improvement of all instruments combined is $\Delta\chi^2 = 139.88$.

As can be seen in the left panels of Fig. 4, the non-corrected residuals show the same shape as the Crab and 3C 273 data, with a clear bump around 8 keV. Note also that the *NuSTAR* residuals show almost the opposite shape to the EPIC-pn residuals, creating an "X"-shape. As expected this shape is strongly reduced when using the new CCF (Fig. 4, right panels).

Individual observation typically do not show such a significant improvement, which can be mainly attributed to the lower S/N. In fact, the improvement on average is only $\Delta\chi^2 = 3.0$ for EPIC-pn alone and some spectra result in a worse fit with the new CCF (see Table 4). We ascribe this to random fluctuations and imperfect modelling. In particular, if the *NuSTAR* data are not very constraining, we might find a model that describes the non-corrected data very well, modelling the "bump" as part of the model. This model, however, might not describe the underlying spectrum correctly (or physically) and hence cannot describe the corrected data as well.

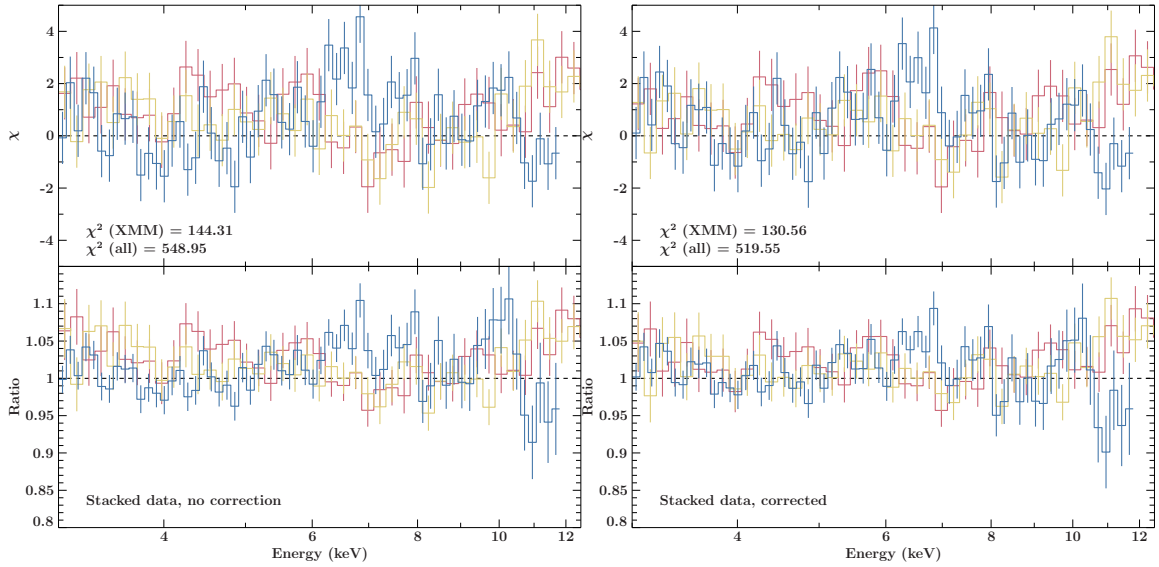

Figure 5: Same as Fig. 4 but for 35 full-frame observations. Given the lower S/N of the data, the improvement is not as clear as for the small window mode observations.

3.2 Full Frame mode

We also tested the correction function on 35 simultaneous observations during which EPIC-pn was operated in the full frame mode (Table 5). We only selected observation with a prominent point source close to the optical axis, and extracted the source spectra from a circular region of typically 30″ radius. For brighter sources, we increased the radius to up to 45″. We checked for pile-up and extracted an annulus, excluding the inner region where necessary, which was the case for two sources (ObsID 0800350201 of M33 FIELD-2 and ObsID 0692790201 of Cen X-4). We also checked if it is necessary to enforce strict simultaneity between *XMM-Newton* and *NuSTAR* by examining the variability of the light-curve. We found that it is necessary for five sources (ObsIDs 0692790201, 0800350201, 0841800201, 0800030901, and 0803990101) while all others showed very little to no variability.

Overall, the the source types are more varied in this sample compared to the small-window AGN sample described in the previous Section. However, all sources are much fainter than the small-window targets and have therefore only a limited S/N. As before, we fitted the data with simple phenomenological models, typically consisting of a power-law and a thermal blackbody component.

Figure 5 shows the results of this sample. We again find an overall improvement when using the correction function, however, it is much smaller than in the case of the small window observations ($\Delta\chi^2 = 11.44$ for EPIC-pn only and $\Delta\chi^2 = 13.22$ for all data together).

3.3 SED of 1ES 0229+200

One of the main drivers for selecting 1ES 0229+200 as an additional calibration source was the intriguing possibility to be able to connect the UV fluxes, as measured by the Optical Monitor (OM) directly to the X-ray fluxes. This would provide another way to directly test the absolute flux calibration of EPIC-pn, as the UV fluxes are very well calibrated based on UV standards (Rosen, 2020). Wierzcholska & Wagner (2020) showed that this connection is very clear in the archival data taken in 2013, when allowing for slightly increased absorption on the X-ray flux.

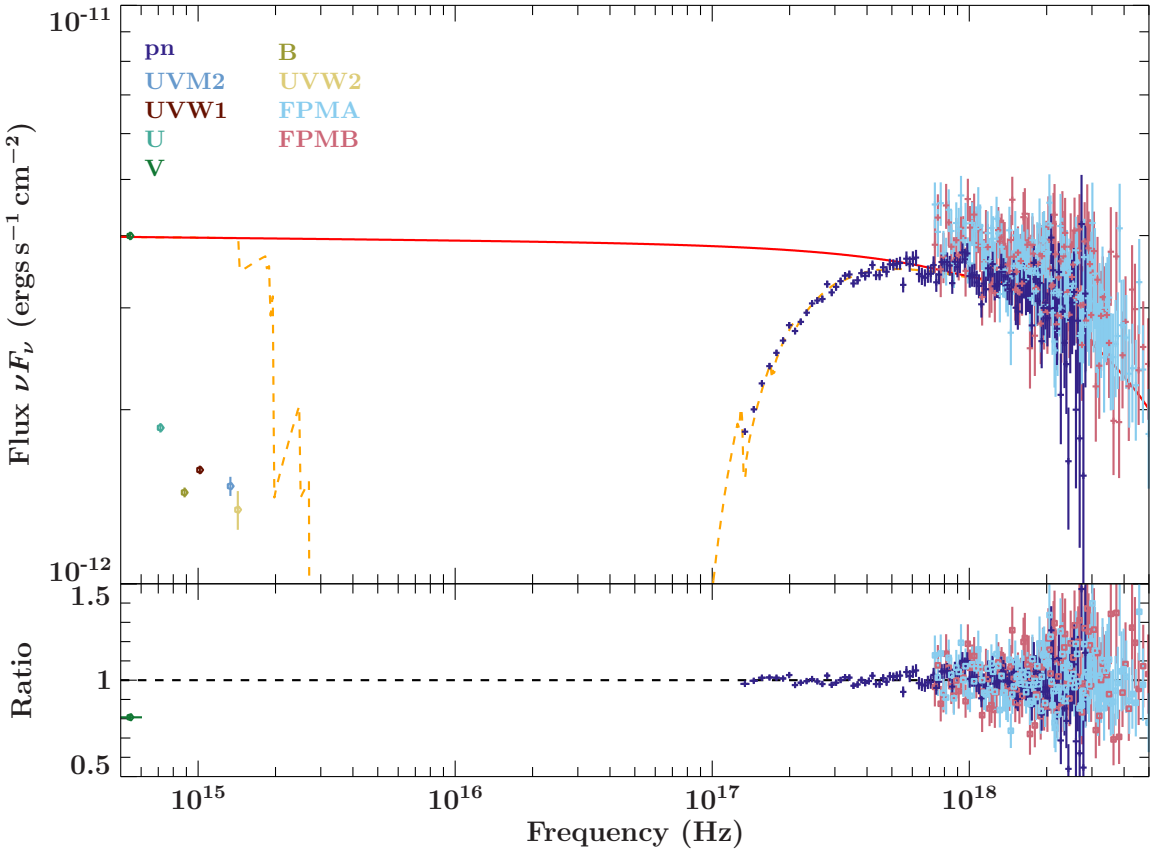

Figure 6: OM, EPIC-pn (blue), and *NuSTAR* (weird colors) data of 1ES 0229+200 during the 2021 calibration observation. The red model is the best-fit model to the X-ray data, evaluated without the absorption, while the orange dashed line shows the best-fit X-ray model with the fitted absorption column. As can be seen, the extrapolation to the UV band drastiaclly overestimates the UV flux. The V band is influenced by the host galaxy and therefore not represenattive of the AGN.

We therefore performed observations with the V, B, U, UVW1, UVM2, and UVW2 filters during the calibration observation in 2021. We carefully checked that the data are not affected by stray light or the "Jupiter patch" (Rosen, 2020). Overall, we find the fluxes to be very similar to the data taken in 2013, e.g., with a flux of $2.735 \times 10^{-12}\,\mathrm{erg\,s\,cm^{-2}}$ in the UVW2 band.

However, the X-ray flux was much lower in 2021 compared to 2013 ($\mathcal{F}_{2021} = (5.18 \pm 0.08) \times 10^{-12}\,\mathrm{erg\,s\,cm^{-2}}$ compared to $\mathcal{F}_{2013} = \left(9.73^{+0.19}_{-0.23}\right) \times 10^{-12}$ in the 3–20 keV band) and at the same time the source softened significantly ($\Gamma_{2021} = 1.989 \pm 0.023$ compared to $\Gamma_{2013} = 1.784^{+0.017}_{-0.046}$). This leads to a dramatic overstimation of the UV flux based on the best X-ray model, see Fig. 6.

It therefore seems that the proposed connection between the UV flux and the X-ray flux does not hold during the low states of 1ES 0229+200 and hence cannot be used as another calibration anchor point. Nonetheless, given its simple spectral shape, 1ES 0229+200 is a useful source to perform cross-calibration between different X-ray instruments.

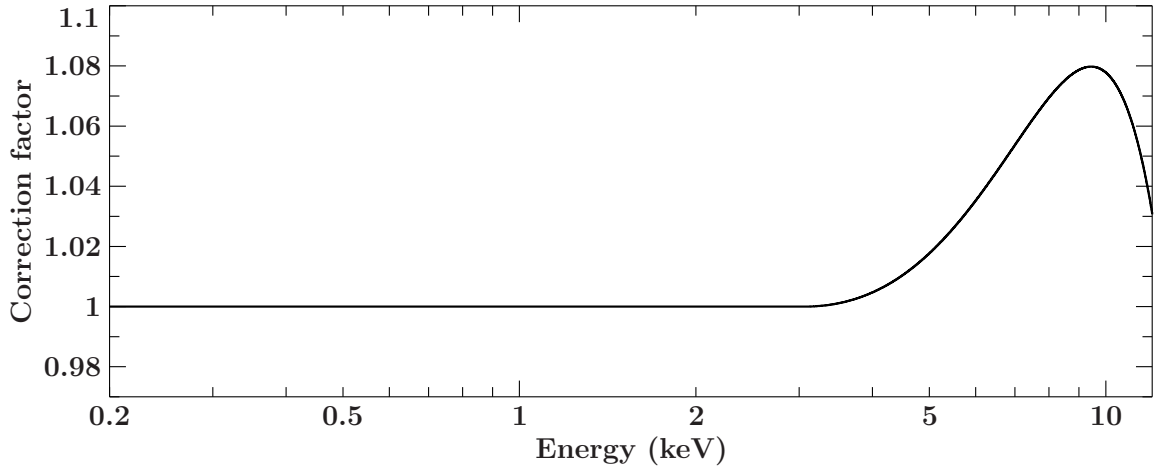

Figure 7: Final correction function to the EPIC-pn ARF description, taking into account the slope and shape difference to *NuSTAR*, as well as the offset to the absolute normalization. These values are published in the `ABSCORRAREA` extension of `XRT3_XAREAEF_0014.CCF`.

4 Summary & Results

We have used data of the Crab taken by *XMM-Newton* and *NuSTAR* simultaneously over the last ~ 8 years to update the description of the EPIC-pn ARF and provide a better agreement with the *NuSTAR* spectral shape. We find that by applying a spline function to the EPIC-pn data between 3–12 keV with maximum relative change of 5% significantly improves the agreement with *NuSTAR* for both sources. In addition, we have used observations of 3C 273 and 1ES 0229+200 by *XMM-Newton* and *NuSTAR* to confirm the proposed changes. In these data we also find that the EPIC-pn fluxes are lower by about 20% compared to the *NuSTAR* fluxes, which users should keep in mind when working with simultaneous observations. We recommend to use a free cross-calibration constant between EPIC and other instruments to correct for this discrepancy.

We have tested the correction function with a sample of 22 AGN observed in small window mode and 35 more sources taken in full-frame mode, observed simultaneously between *XMM-Newton* and *NuSTAR* and find a significant improvement in the stacked residuals and quality of fit.

We provide the new CCF `XRT3_XAREAEF_0014.CCF` which includes the corrections presented here. The corrections can be activated in SAS 20.0 and later versions by setting `applyabsfluxcorr=yes` in `arfgen`. While the corrections are calculated based on EPIC-pn data, they will also be applied to MOS data to avoid any artificial differences between the cameras. Details about the new CCF file are described in the CCF release note XMM-SOC-CAL-SRN-0388.

5 Outlook & Caveats

The current corrections are based on a limited sample of simultaneous observations. It would be good to test them against a larger sample of dedicated calibration observations of various targets, preferably of targets with simple spectra to eliminate as much as possible modelling uncertainties of the astrophysical processes. Given the requirement for simultaneous observations with *NuSTAR* and targets with sufficient S/N, tests for other EPIC-pn modes (large window, extended full frame) have not yet been performed. Nonetheless, the correction should be applicable to those modes as well.

The corrections are only applicable above 3 keV, where simultaneous data with *NuSTAR* are available. At lower energies more complicated detector physics influence the necessary corrections (see Dennerl et al., in prep.) and no attempt to correct the ARF in this energy range has been made here.

6 References

References

Foreman-Mackey D., Hogg D.W., Lang D., Goodman J., 2013, PASP 125, 306

García J., Dauser T., Reynolds C.S., et al., 2013, ApJ 768, 146

Gokus A., 2017, *Master's thesis*, Friedrich-Alexander-Universität Erlangen-Nürnberg, Remeis-Sternwarte Bamberg

Gokus A., Schartel N., Santos-Lleo M., et al., 2016, In: Active Galactic Nuclei: What's in a Name?, p. 91

Goodman J., Weare J., 2010, Comm. Appl. Math. and Comp. Sci. 5, 65

Houck J.C., 2002, In: G. Branduardi-Raymont (ed.) High Resolution X-ray Spectroscopy with XMM-Newton and Chandra.

Kirsch M.G.F., Schönherr G., Kendziorra E., et al., 2006, A&A 453, 173

Kuster M., Benlloch S., Kendziorra E., Briel U.G., 1999, In: Siegmund O.H., Flanagan K.A. (eds.) EUV, X-Ray, and Gamma-Ray Instrumentation for Astronomy X, Vol. 3765. Society of Photo-Optical Instrumentation Engineers (SPIE) Conference Series, p.673

Madsen K.K., Beardmore A.P., Forster K., et al., 2017a, AJ 153, 2

Madsen K.K., Forster K., Grefenstette B.W., et al., 2017b, ApJ 841, 56

Madsen K.K., Fürst F., Walton D.J., et al., 2015, ApJ 812, 14

Rosen S., 2020, XMM-Newton Calibration Documentation CAL-TN-0019

Verner D.A., Ferland G.J., Korista K.T., Yakovlev D.G., 1996, ApJ 465, 487

Wierzcholska A., Wagner S.J., 2020, MNRAS 496, 1295

Wilms J., Allen A., McCray R., 2000, ApJ 542, 914

7 Appendix

Additional plots and observation log tables.

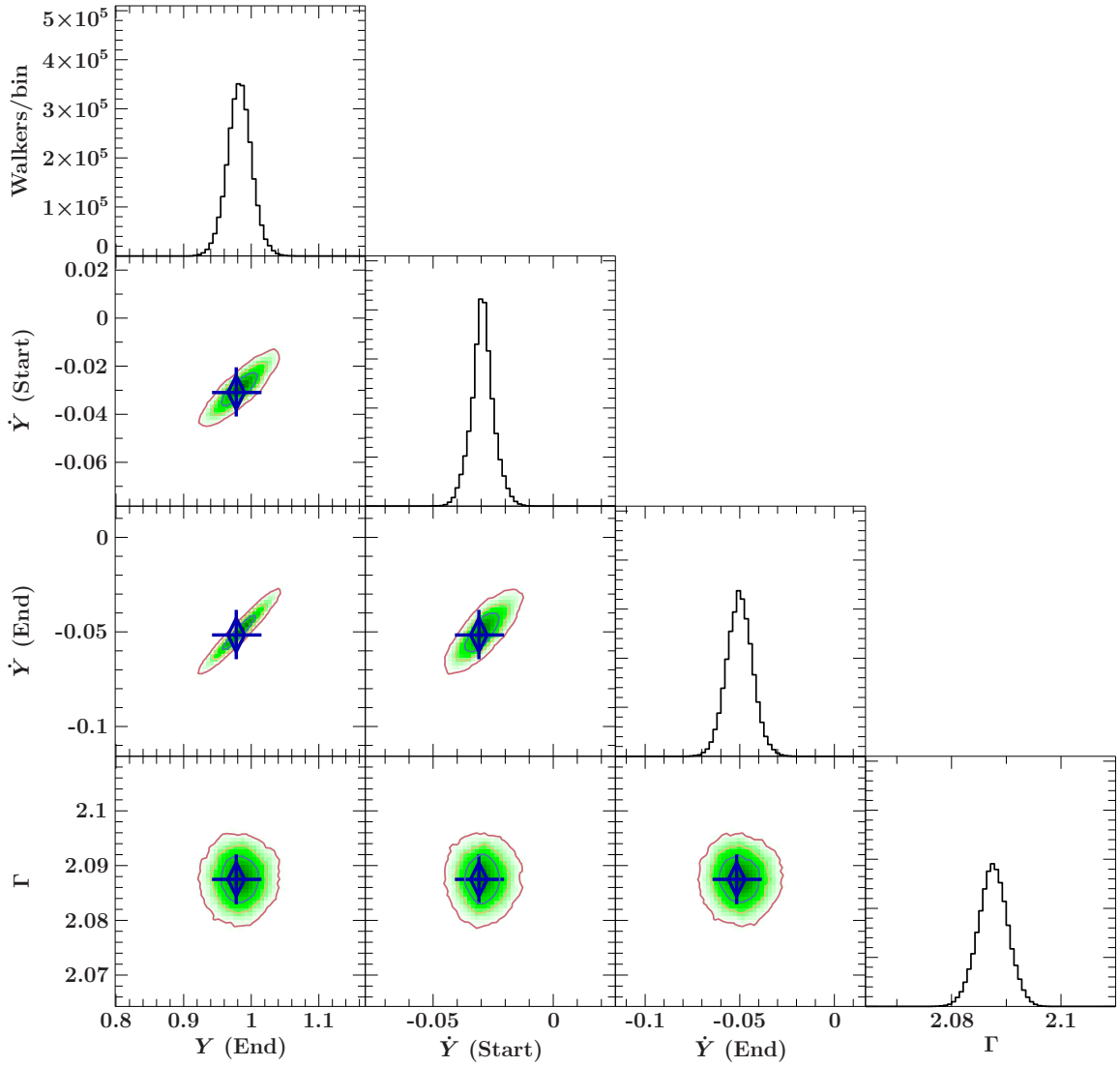

Figure 8: Triangle plot for the relevant parameters of the spline correction function and the photon index Γ for the first epoch (ObsIDs 0414191001 and 1000202001). As can be seen, there is a small degeneracy between Y(End) and $\dot{Y}$(End), but all parameters are very well constrained. The contour levels indicate the 68% (blue), 90% (orange), and 99% (red) confidence level.

Table 4: List of observations used to test the new correction function. All EPIC-pn data were taken in Small Window mode. The last two columns give the best-fit χ^2 value for the uncorrected (base) and corrected data, respectively.

Source	XMM ObsID	NuSTAR ObsID	$\chi^2_{\rm base}$	$\chi^2_{\rm corr}$
NGC 4593	0740920401	60001149006	215.63	216.78
3C120	0693781601	60001042002	286.93	297.18
HE 1136-2304	0741260101	80002031003	222.71	215.87
MCG-6-30-15	0693781401	60001047005	257.04	257.32
HE 1143-1810	0795580101	60302002002	252.38	248.32
HE 1143-1810	0795580201	60302002004	238.57	228.79
HE 1143-1810	0795580501	60302002010	243.22	236.48
Fairall9	0741330101	60001130003	323.62	316.04
MCG-6-30-15	0693781201	60001047002	227.76	219.19
MR2251-178	0763920701	60102025006	263.57	252.70
MR2251-178	0763920801	60102025008	263.70	242.44
MR2251-178	0763920601	60102025004	245.60	234.60
HE 1143-1810	0795580301	60302002006	259.77	256.14
Swift J2127.4+5654	0693781701	60001110002	236.79	230.14
RXS J1131-1231	0820830101	60401001002	230.41	230.79
Swift J2127.4+5654	0693781901	60001110007	291.14	284.86
MCG-6-30-15	0693781301	60001047003	274.36	254.56
IRAS 09149-6206	0830490101	60401020002	190.32	196.22
ESO511-G030	0852010301	60502035006	239.79	232.78
NGC4151	0679780301	60001111005	315.93	308.40
Mrk359	0830550901	60402021004	231.18	228.56
3C382	0790600201	60202015004	285.77	274.95

Table 5: List of observations used to test the new correction function. All EPIC-pn data were taken in Full Frame mode. All spectral fits correspond to the brightest source in the field of view for any given observation. The last two columns give the best-fit χ^2 value for the uncorrected (base) and corrected data, respectively.

Target	XMM ObsID	NuSTAR ObsID	$\chi^2_{\rm base}$	$\chi^2_{\rm corr}$
NGC 1313	0693851201	30002035004	247.55	241.06
IRAS 00521-7054	0795630201	60301029004	242.55	242.55
NGC 4579	0790840201	60201051002	237.82	240.79
CEN X-4	0692790201	30001004002	157.64	156.38
HOLMBERG II X-1	0724810301	30001031005	157.97	158.08
NGC 7090 ULX2	0852050201	80501321002	151.11	151.93
M33 FIELD-2	0800350201	50310002003	150.70	150.57
NGC 1313	0693850501	30002035002	172.35	171.54
M33 FIELD-1	0800350101	50310001004	205.71	204.93
RX J0134.2-4258	0841800201	60501005002	149.98	149.42
ELIAS 29	0800030901	30301001004	151.76	150.01
NGC 1313 X-1	0803990101	30302016002	218.58	218.63
NGC7793 P13	0804670301	30302005002	196.21	193.75
MKN 335	0780500301	80201001002	224.87	223.42
NGC 1313 X-1	0803990601	30302016010	223.06	226.62
HESS J1713-381	0790870201	30201031002	171.40	174.49
IRAS 13197-1627	0763220201	60101020002	312.60	314.37
NGC7793 P13	0804670701	30302005004	178.93	174.06
NGC 1313 X-1	0794580601	90201050002	189.45	191.18
NGC 1313 X-1	0742590301	80001032002	184.97	189.07
NUSTARJ150645+0346.2	0795670101	60301023002	212.49	205.56
NGC 1052	0790980101	60201056002	229.61	227.57
NGC 1194	0852200101	60501011002	248.79	251.82
NGC5907 ULX1	0729561301	80001042002	180.99	183.14
ESO 112-G006	0852180101	60561038002	178.58	178.68
CGCG 475-040	0852181001	60561047002	239.28	240.21
NGC 3081	0852180701	60561044002	288.39	282.98
MGC-07-03-00	0852180201	60561039002	198.14	199.47
ESO 426-G002	0852180301	60561040002	229.07	229.41
NGC 5907 ULX-1	0804091101	30302004008	209.10	206.79
ESO 565-G019	0852180601	60561043002	209.15	208.77
NGC 4785	0743010101	60001143002	206.46	208.11
NGC 6552	0852180901	60561046002	206.08	205.99
ESO 116-18	0795680201	60301027002	227.13	222.70
CXOJ022727.5+333443	0784510301	30201003002	191.64	194.58